

RSC Advances



This is an *Accepted Manuscript*, which has been through the Royal Society of Chemistry peer review process and has been accepted for publication.

Accepted Manuscripts are published online shortly after acceptance, before technical editing, formatting and proof reading. Using this free service, authors can make their results available to the community, in citable form, before we publish the edited article. This *Accepted Manuscript* will be replaced by the edited, formatted and paginated article as soon as this is available.

You can find more information about *Accepted Manuscripts* in the [Information for Authors](#).

Please note that technical editing may introduce minor changes to the text and/or graphics, which may alter content. The journal's standard [Terms & Conditions](#) and the [Ethical guidelines](#) still apply. In no event shall the Royal Society of Chemistry be held responsible for any errors or omissions in this *Accepted Manuscript* or any consequences arising from the use of any information it contains.

Enhancing sorption performance of surfactant-assistant CaO nanoparticles

Aminul Islam^{a, b}, Siow Hwa Teo,^{a, b} Eng Seng Chan,^c Yun Hin Taufiq-Yap^{a, b*}

^a Catalysis and Science Research Center, Faculty of Science, University Putra Malaysia, 43400, UPM Serdang, Selangor, Malaysia.

^b Department of Chemistry, Faculty of Science, University Putra Malaysia, 43400, UPM Serdang, Selangor, Malaysia.

^c Chemical Engineering Discipline, School of Engineering, Monash University, Bandar Sunway, Selangor, Malaysia.

*Corresponding author: Yun Hin Taufiq-Yap
Catalysis Science and Technology Research Centre,
Faculty of Science, Universiti Putra Malaysia, 43400,
UPM Serdang, Selangor, Malaysia.
Tel: +603-89466809, Fax: +603-89466758,
Email: taufiq@upm.edu.my

Abstract

Microsized calcium oxide prepared via precipitated and thermally decomposed from calcium carbonates have been widely used in industrial hydrogen production and biomass gasification process to remove CO₂ from the reactor. One of the most interesting perspectives in catalysis is the development of nano-sized, high performance, and low cost catalyst. However, due to the high cost of nano-sized calcium oxide (CaO), it is critically important to develop a technique that achieves this point of view. The main goal of this study was to prepare zwitterionic surfactant (BS-12) modified nano-calcium oxide sorbent. The *Ctenocardia fornicata* shell was used as a precursor of nanoCaO, as it is cheap and easily available. The effect of BS-12 on the physico-chemical properties and the performance of nano CaO sorbent for capturing CO₂ were investigated. Thermo gravimetric analysis (TGA), X-ray diffraction (XRD), fourier transformer infra-red (FT-IR), X-ray fluorescence (XRF), N₂ adsorption/desorption (BET), transmission electron microscope (TEM), zeta potential and temperature programmed desorption (TPD-CO₂) were used for the characterization of the prepared nano-sized CaO particles. The results showed that the BS-12 modified nano-CaO exhibited the best performance for CO₂ capture. The particle sizes and morphologies of CaO varied from rod shape (45–33 nm) to cubic (13-23 nm) with changing the operating variable. The suggested mechanism for nanoparticle formation in presence of BS-12 was also discussed.

Keywords: Nano-sized CaO; surfactant; BS-12; morphology; size.

Introduction

In combating climate change, CO₂ capture and storage (CCS) using various CO₂ absorbents represents the sole effective solution to reduce such a huge scale of CO₂. The emissions of CO₂ can be reduced by CO₂ capture in industrial hydrogen production processes such as coal gasification, methane steam reforming, water gas shift reaction and biomass gasification.¹ In addition to the environmental impact, CO₂ removal from the reactor in biomass gasification process improves volatilisation and gasification steps shifting the balance towards the hydrogen production.² CO₂ is captured in the form of CaCO₃. Though, the carbonation and calcination reactions are not totally reversible. It is related to conditions as temperature and pressure,³ as follows:

$$P_{CO_{2eq}}(\text{atm}) = 4.137 \times 10^7 \times \exp\left(-\frac{20,474}{T(\text{K})}\right)$$

Indeed, calcium oxide (CaO) readily obtained through the calcination of naturally occurring sea shell has been proposed as an alternative CO₂ sorbent that could substantially reduce the costs of CO₂ capture. Thus, the benefits associated with the use of nano calcium carbonate (CaCO₃) as CaO based precursor can be expected to create positive breakthrough.

There are very few reports on the preparation of CaO in nano size range. Koper *et al.*⁴ (1997) and Tang *et al.*⁵ both used a sol-gel method to prepare nano CaO from calcium methoxide (Ca(OCH₃)₂) precursor and calcium nitrate (Ca(NO₃)₂·4H₂O), respectively. Recently, Amin Alavi and Morsali⁶ used a sonochemical method to synthesize CaO from calcium acetate and nanoparticle tetramethylammonium hydroxide precursors. More recently, Roy and Bhattacharya⁷ performed a microwave irradiation technique to synthesize nano CaO particles using Ca(NO₃)₂·4H₂O and NaOH. However, the cost associated raw materials is one of the drawbacks of these processes. While other studies have investigated the effect of surfactant type on the crystallization and polymorphic transition of emulsified particles,^{8,9,10,11} a study of the effect of zwitterionic surfactant on nanoparticle formation and their

performance for CO₂ capture have to the best of our knowledge, not yet been conducted. The *Ctenocardia fornicata* shell was used as a precursor of nano CaO, as it is cheap and easily available. The suggested mechanism for the nanoparticle growth in presence of surfactant was also discussed.

Experimental

Materials

Waste *Ctenocardia fornicata* shell was collected from Port Dickson beach, Negeri Sembilan, Malaysia. Dodecyl dimethyl betaine (BS-12) was purchased from Sigma-Aldrich (Steinheim, Germany). The deionized water used was HPLC-grade of resistance >18 MΩ obtained from a Milli-Q-Water System (Organex). All of the chemical reagents used were analytical grade in this experiment.

Sorbent preparation

The nano-sorbent CaO was prepared from *Ctenocardia fornicata* shell. The shells were washed with deionized water to remove dirt and dried at 110 °C in the oven for 2 h. Then, the shells were finely grounded using a blender (Blendor, HCB 550, USA). The powders were sieved using a stainless laboratory test sieve with an aperture size of 250 μm (Endecott Ltd., London, England) to obtain micron-sized powders. In a typical procedure, 10 g of micron-sized *Ctenocardia fornicata* shell powder was stirred with 100 mL deionized water in a conical flask to form a colloidal solution. The pH of the solution was adjusted 6.4-6.5 to facilitate decomposition of CaCO₃.¹² Subsequently, BS-12 (4 %) was added into the colloidal solution and adjusted the pH to 13.5 with 10N NaOH. The resulting colloidal solutions were then stirred (1000 rpm) for 30 (S1), 60 (S2), 90 (S3) and 120 (S4) min at room temperature. The obtained samples were separated using a double ring filter paper and dried at 100 °C in the oven for 24 h. Finally, the dried samples were calcined at 850 °C for 4 h. The calcined

samples were labelled as C1, C2, C3 and C4, donated as stirring time intervals of 30, 60, 90 and 120 min, respectively.

Sorbent characterization

Thermogravimetric

Thermogravimetric analysis (TGA) of the waste cockle (*Ctenocardia fornicata*) shell powder was employed on a Mettler Toledo thermogravimetric analyser. The analysis was performed in a nitrogen atmosphere over a temperature range of 35-1000 °C at a heating rate of 10 °C min⁻¹.

Structure and crystallography

X-ray powder diffraction (XRD) analysis of the sample was carried out using a Powder X-ray diffractometer (Shidmazu Corporation, Japan) model XRD 6000 in reflection mode with Cu K α radiation. The Cu K α radiation was generated by a Philips glass diffraction X-ray tube (broad focus 2.7 kW type).

Surface functional group

The surface functional group of the sample was ascertained using attenuated total reflection-Fourier transform-infrared (FT-IR) on a Perkin Elmer (PC) Spectrum 100 FTIR spectrometer. The FT-IR spectra were obtained over the region 400-4000 cm⁻¹ with spectral resolution of 4 cm⁻¹.

Elemental analysis

The chemical composition of the sample was determined by energy dispersive X-ray fluorescence (XRF) spectrometer using Bruker AXS. The metal concentration in the examined samples was determined by the amount of emitted X-ray radiation related to the values in the calibration curves.

Specific surface area

The BET specific surface area of the sample was measured by the Brunauer Emmett and Teller (BET) method using nitrogen adsorption at $-196\text{ }^{\circ}\text{C}$. The analysis was conducted using a Surfur, Thermo Scientific instrument.

Morphology

The morphological observation of the sample was made by Transmission Electron Microscopy (TEM, Hitachi, H7100). TEM specimens were prepared by depositing a few drops of sample dispersed in ethanol on carbon coated copper grid. Particle size of the sample was obtained by using TEM with an accelerating voltage of 200 kV.

Surface charge analysis

Zeta potential measurement was performed by a 3000 HSA analyzer (Malvern). The suspension was made by the self-dispersed powder in methanol. Light scattering was monitored at a 90° scattering angle and a temperature of $25\text{ }^{\circ}\text{C}$ in a clear disposable cell.

Sorbent sorption capability

The absorption test of the sorbents was carried out with by CO_2 pulse chemisorption and temperature programmed desorption (CO_2 -TPD) analysis. Both experiments were performed using a Temperature Programmed chemisorption/desorption (Thermo Finnigan TPDR0 1000) apparatus equipped with a thermal conductivity detector (TCD). Prior to the pulse chemisorption experiment, 200 mg of synthesized sorbent was pretreated at $750\text{ }^{\circ}\text{C}$ for 30 min under helium stream ($10\text{ }^{\circ}\text{C min}^{-1}$, 20 mL min^{-1}) in order to desorb CO_2 and moisture molecules that come from atmosphere air, and then the temperature was maintained at $750\text{ }^{\circ}\text{C}$. Subsequently, the measurement of CO_2 absorption was recorded continually during the entire process at $750\text{ }^{\circ}\text{C}$ under a pure CO_2 gas (20 mL min^{-1}) for 1 h. The absorption of CO_2 on the sorbent was evaluated from the peak areas detected by TCD.

For CO₂-TPD measurement, the 200 mg of sorbent was treated at its calcination temperature (850 °C) under the helium flow rate of 30 mL min⁻¹ for 1 h, and saturated with a pure CO₂ flow (30 mL min⁻¹) after cooling to 60 °C. Then, it was flushed with helium (30 mL min⁻¹) to remove the weakly physisorbed CO₂. Consequently, the was proceed at temperature between 50-900 °C under helium (10 °C min⁻¹, 30 mL min⁻¹) as carrier gas and hold for 10 min. Afterward, the CO₂ desorption signal was recorded by TPD with linear temperature increased up to 900 °C at rate of 10 °C min⁻¹. The area of desorption profiles were obtained and the total desorption of CO₂ at 900 °C is then equivalent to the total CO₂ that could be absorbed in the sorbent.

Results and discussion

Previous studies have reported that the addition of surfactant can inhibit crystal growth due to the formation of energy barrier by the surfactant at the solid-liquid interface.¹³ It should be point out that any of the atoms in the nanoparticles can act as the absorber atom.¹⁴ A strong absorption of surfactant at the nanoparticle growth site would reduce the growth rate of nanoparticles, has been reported by Mehta *et al.*¹⁵ although, Sajanlal *et al.*¹⁶ concluded from their work that the full coverage of surfactant would hinder the diffusion of growth species from the surrounding solution to the surface of growing particles. Hence, synthesis of CaO nanoparticles from *Ctenocardia fornicata* shells using surfactant-assistant precipitation approach has been proposed in this study. Tai *et al.*¹⁷ in their discussion of the decomposition properties of calcium carbonate have emphasized the influence of pH on the decomposition. A similar conclusion has been reached by Han *et al.*¹² who reported that the decomposition of CaCO₃ could be facilitated at the pH of below 6.5. It might be noted that the zwitterionic surfactant (BS-12) used in this study possess polar head groups which on ionisation imparts both positive and negative charges at the isoelectric point. As the pH shifts away from the isoelectric point to 13.5, the molecule of surfactant behaves as properties of anionic

surfactant.¹⁸ Thus, the precipitation of calcium carbonate could take place at this pH due to the electrostatic repulsion interaction between the anionic surfactant and the anionic carbonate ions. Finally, CaO sorbent was produced via thermal decomposition of precipitated calcium carbonate. As indicated earlier, the objective of this present work was to compare the sorption performance of surfactant-assistant CaO nanoparticles, and this, in turn, required the preparation of well-characterized CaO nanoparticles.

Thermal decomposition of sorbents

The *Ctenocardia fornicata* shells were analyzed by TGA for determining decomposition temperature of shells. Fig.1 shows TGA curves for the *Ctenocardia fornicata* shell and treated shells. The thermogram (Fig.1a) of shell shows two weight lost steps with a total weight loss of 56.7%. A single major weight loss peak was observed from TGA curve at a temperature range of 600-800 °C (47%), could be attributed to the decomposition of CaCO₃ into CaO. This is in agreement with those reported by Sivakumar *et al.*¹⁹ The weight of the sample was remained constant at above 850 °C. Therefore, complete temperature occurred at temperature above 850 °C is required to transform CaCO₃ to CaO as follows:



Fig.1b-e shows that the initial decomposed temperature of treated shells reduced gradually, which suggested that the grain size of the treated shell was reduced by the treatment of surfactant. Archer Jr *et al.*²⁰ studied the thermal decomposition kinetics of calcium carbonate and reported that the decomposition of CaCO₃ at lower temperature is the signature of small particle-sized. Further, it has been argued by Zuiderduin *et al.*²¹ that the larger particles require a higher decomposition temperature than the small particles.

Structure of sorbents

The XRD patterns of *Ctenocardia fornicata* shell shown in Fig. 2a suggest the presence of CaCO₃ phase without any additional diffraction peaks at 2θ values of 26.3°, 27.3°, 31.2°, 33.1°, 36.2°, 37.9°, 38.7°, 41.3°, 43.0°, 45.9°, 48.4°, 50.2°, 52.5°, 53.1°, 66.2° and 69.0° (JCPDS file: 01-071-2396). Diffraction patterns of treated shell (S-4) were exhibited similar to Fig. 2a. The XRD profiles of sorbents (Fig.2c-f) corresponds to the characteristic CaO peaks at 2θ values of 32.1°, 37.3°, 53.8°, 64.1°, 67.3° and 79.6° (JCPDS file: 00-037-1497). No peaks from any other phases of CaO were observed. The results indicate that the thermal decomposition of CaCO₃ in powder shell convert into CaO, which agrees with the results from the literature.^{19,22} Although the peak positions in the XRD pattern in Fig. 2c-f are similar, the XRD peaks of these compounds gradually appear broader suggesting the decrease of crystallite size.²³

Surface functional group of sorbents

The FTIR spectra of *Ctenocardia fornicata* shell, treated shell and sorbents (C1-C4) are presented in Fig. 3 and Table 1. The IR spectrum of the shell (Fig. 3a) at 1455, 857 and 712 cm⁻¹ are characteristic of the C–O stretching and bending modes of calcium carbonate.²⁴ In addition, the weak band that appeared at 1794 cm⁻¹ is assigned to an overtone or combination of some vibrational modes of divalent metal ions and carbonate groups bond. Although the absorption peaks of the surfactant treated shell (Fig. 3b) are similar, the existence of alkyl groups at 2983 and 2533 cm⁻¹ are due to hydrophobic tail of surfactant formed during treatment. Fig. 3c-f shows the spectrum of the calcined treated shell. The results shows that the spectrum of the all CaO sorbents (Fig. 3c-f) appeared at the same wave number, indicating that they have a very similar chemical nature. The existence of peak at 3640 cm⁻¹ is due to OH in Ca(OH)₂ formed during adsorption of water by CaO. The wide and strong band at around 500 cm⁻¹ corresponds to the Ca–O band.

Composition of *Ctenocardia fornicata*

The XRF analysis result (Table 2) confirmed that the composition of *Ctenocardia fornicata* shell mainly consists of Ca (99.9 %). The high amount of Ca is associated with the presence of CaCO₃, which is the main component of the shell confirmed by the XRD and FTIR results. The shell contains small amounts of S, K, Sr, Cu and Fe. Thus, the shell can be considered from a chemical viewpoint as a pure relatively natural carbonate-based material.

Surface charge of calcium carbonate

Fig. 4 and Table 3 show the zeta potentials of *Ctenocardia fornicata* shell and treated shell (S4). It can be observed that, zeta potential of BS-12 treated sample (S4) at pH 6.4 is -20.13.4 mV (Fig. 4a), whereas, this value decreased to -4.13 mV at pH 13.5 (Fig. 4b). Thus, the results revealed that BS-12 neutralized the surface charge CaCO₃ at 13.5 and the zeta potential approached to zero.

Size and morphology of sorbents

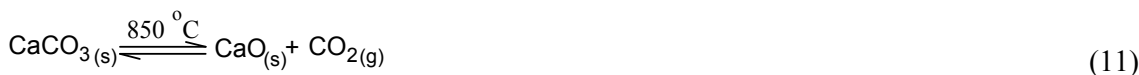
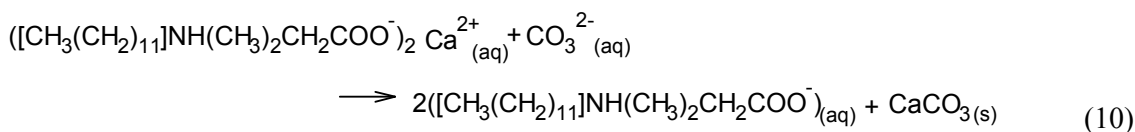
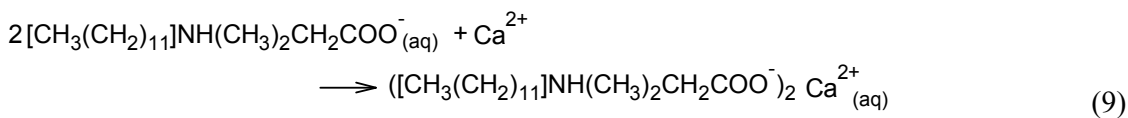
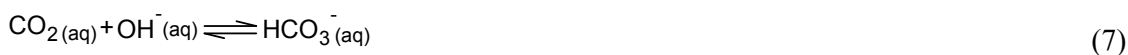
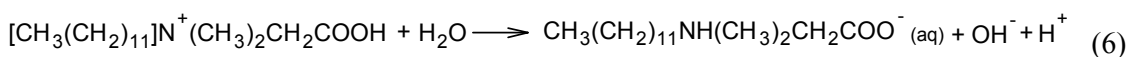
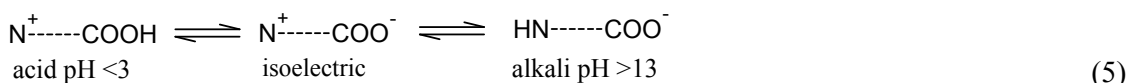
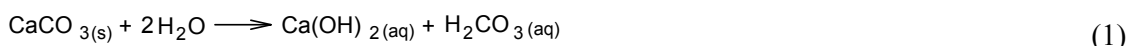
Fig. 5 shows the representative TEM images of the sorbents. The rod-shaped CaO nanoparticles with a diameter of about 33-45 nm are predominant after 30 min of retention time (Fig. 5a), while the regular and spherical in shape with a particle size of 30-37 nm are prevailing over a time course of 60 min (Fig. 5b). When the reacting time is up to 90 min, the size of spherical particle is reduced to 30-24 nm (Fig. 5c). Further increasing a period of time up to 120 minutes, smaller nanoparticles can be obtained (Fig. 5d) and the average diameter of the CaO nanorods is about 13-23nm. The produced particles have narrow size of distribution and limited amount of agglomerate. The results reveal that the surfactant treated at different time intervals affect the shape and size of the CaO nanoparticle. It has been reported by El-Sheikh *et al.*²⁵ that the surfactant molecules attach to the solid particle and form a layer between the particle and the surrounding fluid molecules. Such layers impart a

repulsive force between them and in turn, prevent particle aggregation. A conclusion has been reached by Tanvir and Qiao²⁶ that the surfactant increases the electrostatic force of solid-liquid interface and thus reduces the aggregation of particles. A similar observation has been made by Helgason *et al.*²⁷ who investigated the impact of surfactants on the rate of crystal growth of solid lipid nanoparticles. Further, it has been shown by other workers²⁸ that the strong adsorption of surfactant would occupy the nanoparticle growth's site, thus reducing the growth of particles. Thus, the formation of nanoparticles observed in this study seems to be indicative of a nucleation sensitive phenomenon which is presumably an inherent feature of the zwitterionic surfactant (BS-12). Therefore, the presence of zwitterionic surfactant beside a large number of CaCO₃ nucleation, in the initial period of carbonation reaction controls the rate of the crystal growth and then the monodisperse CaCO₃ nanoparticles were successfully prepared.

Proposed mechanism

The main ingredient in *Ctenocardia fornicata* shell is CaCO₃ which was confirmed by XRD, FTIR, XRF and TGA analyses. Calcium carbonate aqueous solution pH value is 8.0~8.6. The pH of the solution was adjusted below 6.5 to facilitate decomposition of CaCO₃ (Eq. 1-4).¹² Han *et al.*¹² reported that the reaction of Eq.3 is slower than reaction of Eq. 2. Hence, CaCO₃ is not precipitated at pH < 6.5 due to the absence of sufficient CO₃²⁻ ion in the solution.¹² It is well known that the dodecyl dimethyl betaine (BS-12) is an amphoteric surfactant, containing both cationic and anionic groups (Eq. 5). Addition of BS-12 to the colloidal suspensions of CaCO₃ at pH 13.5, the suspension allowed the BS-12 to dissociate dodecyldimethylaminoacetate (Eq. 6). The dissociation of CaCO₃ at pH 13.5 was reported by Han *et al.*¹² is shown in Eq. 7-8. The reaction of Eq. 8 is faster than reaction of Eq.7 at pH 13.5, which leads to an even higher concentration of CO₃²⁻ than HCO₃⁻ in the solution.¹² Therefore, the precipitation of CaCO₃ can be achieved at pH over 13.5 according to reaction

of Eq 9-10. It may be due to the electrostatic repulsion interaction between the negatively charged alkyl chain and the CO_3^{2-} ion, which makes its adsorption onto the face of CaCO_3 difficult. Finally, calcium oxide is produced via thermal decomposition of calcium carbonate (Eq.11). The suggested mechanism can be confirmed by TGA, XRD, FT-IR, zeta potential and TEM, as shown in Fig. 1, Fig. 2, Fig. 3, Fig. 4 and Fig. 5.



BET specific surface area and porosity of sorbents

Fig.6 presents the N₂ physisorption (adsorption/desorption) isotherms of sorbent. According to the international union of pure and applied chemistry (IUPAC) classification of adsorption isotherm, type II describes the presence of mesopores (2–50 nm pore diameter) and micropores exhibits a hysteresis loop and a variation point at lower pressure (P/P_0) in a material.²⁹ The isotherms have a sharp slope at relative pressure from 0 to 0.1, which can be attributed to the presence of micropores, and a small slope at relative pressure from 0.4 to 0.8, which indicates a broad pore-size distribution in the mesopore range (Fig. 6a-f). However, the surface area of each sample was quite different (Table 4).

The pore size distribution curves, as shown in Figs. 7a-f, demonstrated the uni-modal pore size distribution for all sorbents. The commercial CaO (Fig. 5a) shows mainly exhibits pores of diameter higher than 10 nm while the C1, C2, C3 and C4 (Fig. 7b-f) present a distribution shifted towards smaller pore sizes (> 2 nm). The BET surface area of commercial CaO, C1, C2, C3 and C4 are 4.7, 8.4, 10.8, 13.5 and 23.7 m² g⁻¹ corresponding to average value pore sizes are 10.62, 8.05, 6.23, 6.50 and 2.26 nm, respectively. The results revealed that the surface area of the sorbent is increased as extends periods of time. The C4 shows the highest specific surface area (24 m²/g), which is mainly contributed by mesopores and micropore surfaces. The surface areas (S_{BET} 5-23 m² g⁻¹) reported in Table 4 can be favourably compared with the nano CaO produced from different shell.^{30,31}

Performance of sorbents

CO₂-TPD measurements were carried out to determine the absorption amount of CO₂ in the treated and commercially available CaO sorbents (Fig. 8). The results of the CO₂ absorption test are presented in Table 5. It is obviously that the treated samples have significant differences in CO₂ sorption performance compared to commercially available CaO sorbents. These differences could be partially attributed to the higher BET surface areas on the treated

sorbents compared to commercial sorbents, maximizing the number of available sorption sites for CO₂ absorption. Sun *et al.*³² suggest that the rapid adsorption of CO₂ at the beginning of the process is due to external surface of the adsorbent, and is followed by slower internal diffusion process. According to the model developed by Bouquet *et al.*³³ the first step of carbonation finishes when all the grains are filling and the carbonate layer reaches a critical thickness then in the second step CO₂ must diffuse at the level of the whole grain. Further, it was reported by Lu and Smirniotis³⁴ that the diffusion of CO₂ could be accelerated with decreasing particle size. Thus, the nano-CaO increase an exposed surface area for the surface reaction of CO₂ and decrease the thickness of CaO layer for the CO₂ diffusion. To have an insight into the CO₂ absorption of the sorbents, the desorption test was performed using same batch of the sorbents (Fig. 9) and the results were shown in Table 5. The result shows that the amount of desorbed CO₂ was very close to its amount absorbed. Thus, this result confirms the connection between physical properties of sorbent and absorption/desorption capacities. However, the sorption performance of CaO could be affected by the lattice structure of sorbent, as reported by Ying *et al.*³⁵ Thus, issues related to the lattice structure needs to be addressed in the future.

Conclusions

Nano calcium oxide sorbents having a range of size and morphology were synthesized in this work. The results suggest that the zwitterionic surfactant coverage at the interface of the particle controls the rate of crystal growth and favours the formation of nano calcium oxide. The produced calcium oxide particle's morphology and size are significantly changed from rod shape (45–33 nm) to cubic (13–23 nm) with operating variables. The synthesized nano sorbents were subjected to chemisorption/desorption in presence of CO₂. Sorbents with higher surface area demonstrated larger capacity for the CO₂ chemisorption/desorption. Among all the sorbents, The C4 had the largest capacity for capturing CO₂ due to its smaller

CaO particle size which provides a higher exposed surface for the surface reaction of CO₂. However, the research related to the lattice structure needs to address in future, as it may affect the sorption performance of calcium oxide.

References

- 1 A. A. Olajire, *Energ.*, 2010, **35(6)**, 2610.
- 2 N. H. Florin. and A. T. Harris, *Chem. Eng. Sci.*, 2008, **63(2)**, 287.
- 3 F. Garcia-Labiano, A. Abad, L. F. De Diego, P. Gayan and J. Adanez, *Chem. Eng. Sci.*, 2002, **57(13)**, 2381.
- 4 O. B. Koper, I. Lagadic, A. Volodin and K. J. Klabunde, *Chem. Mater.*, 1997, **9(11)**, 2468.
- 5 Z. X. Tang, D. Claveau, R. Corcuff, K. Belkacemi and J. Arul, *Mater. lett.*, 2008, **62(14)**, 2096.
- 6 M. Amin Alavi, and A. Morsali, *J. Exp. Nanosci.*, 2010, **5(2)**, 93-105.
- 7 A. Roy, and J. Bhattacharya, (2011). *Int. J. Nanosci.*, 2011, **10(03)**, 413.
- 8 H. Bunjes, M. H. Koch and K. Westesen, *J. pharm.sci.*, 2003, **92(7)**, 1509.
- 9 H. Bunjes, F. Steiniger and W. Richter, *Langmuir*, 2007, **23(7)**, 4005.
- 10 T. Awad and K. Sato, *J.Am. Oil Chem. Soc.*, 2001, **78(8)**, 837.
- 11 T. Awad and K. Sato, *Colloids Surf. B*, 2002, **25(1)**, 45.
- 12 S. J. Han, M. Yoo, D. W. Kim and J. H. Wee, *Energ. Fuels*, 2011, **25(8)**, 3825.
- 13 M. M. Fryd and T. G. Mason, *Soft Matter*, 2014, **10**, 4662.
- 14 M. K. Hedayati, F. Faupel and M. Elbahri, *Mater.*, 2014, **7(2)**, 1221.
- 15 S. K. Mehta, S. Kumar, S. Chaudhary and K. K. Bhasin, *Nanoscale Res. Lett*, 2009, **4(10)**, 1197.
- 16 P. R. Sajanalal, T. S. Sreeprasad, A. K. Samal and T. Pradeep, *Nano Reviews*, 2011, **2**, 5883.
- 17 C. Y. Tai, W. R. Chen and S. M. Shih, *AIChE J.* 2006 **52(1)**, 292.
- 18 S. Paria and K. C. Khilar, *Adv. Colloid interface Sci.*, 2004, **110(3)**, 75.

- 19 P. Sivakumar, P. Sivakumar, K. Anbarasu, R. Mathiarasi, and S. Renganathan, *Int. J. Green Energy*, 2014, **11(8)**, 886.
- 20 P. D. Archer Jr., D. W. Ming and B. Sutter, *Planet. Sci.*, 2013, **2(1)**, 1.
- 21 W. C. J. Zuiderduin, C. Westzaan, J. Huetink, and R. J. Gaymans, *Poly.*, 2003, **44(1)**, 261.
- 22 W. Suryaputra, I. Winata, N. Indraswati and S. Ismadji, *Renew. Energy*, 2013, **50**, 795.
- 23 Y. Park, W. J. Lee and H. G. Kim, *J. Phys. Condens. Matter*. 1997, **9(43)**, 9445.
- 24 G. Gergely, F. Wéber, I. Lukács, A. L. Tóth, Z. E. Horváth, J. Mihály and C. Balázs, *Ceram. Int.*, 2010, **36(2)**, 803.
- 25 S. M. EL-Sheikh, S. El-Sherbiny, A. Barhoum, and Y. Deng, *Colloids Surfac. A*, 2013, **422**, 44.
- 26 S. Tanvir and L. Qiao, *Nanoscale Res. Lett.*, 2012, **7(1)**, 1.
- 27 T. Helgason, T. S. Awad, K. Kristbergsson, D. J. McClements and J. J. Weiss, *Colloid Interface Sci.*, 2009, **334(1)**, 75.
- 28 M. Idrees, *Iran. J. Chem. Chem. Eng.* 2013, **32(3)**, 27.
- 29 J. Rouquerol, D. Avnir, C. W. Fairbridge, D. H. Everett, J. M. Haynes, N Pernicone and K. K. Unger, *Pure Appl. Chem.*, 1994, **66(8)**, 1739.
- 30 G. Montes-Hernandez, A. Fernandez-Martinez, L. Charlet, D. Tisserand and F. Renard, *J. Cryst. Growth*, 2008, **310(11)**, 2946.
31. L. Zhao, Z. Qiu and S. M. Stagg-Williams, *Fuel Process. Technol.*, 2013, **114**, 154.
- 32 P. Sun, J. R. Grace, C. J. Lim and E. J. Anthony, *Energy & fuels*, 2007, **21(1)**, 163.
- 33 E. Bouquet, G. Leysens, C. Schönnenbeck and P. Gilot, *Chem. Eng. Sci.*, 2009, **64(9)**, 2136.
- 34 H. Lu and P. G. Smirniotis, *Ind.Eng. Chem. Res.*, 2009, **48(11)**, 5454.
- 35 Z. Ying, H. Jian Ming, C. Quan Zhen, Q. Meia, L. yia, H. Xin and Z. Yong Fan, *Chinese j. struct. chem.*, 2013, **32(11)**, 1715.

Figure of captions:

Fig. 1 TGA analyses of the powdered *Ctenocardia fornicata* shell (a) and treated shells: (b) S1 (c) S2, (d) S3 and (e) S4.

Fig. 2 X-Ray diffraction pattern of (a) *Ctenocardia fornicata* shell (b) treated shell (S4) and sorbents: (c) C1, (d) C2, (e) C3 and (f) C4.

Fig. 3 FT-IR spectra of (a) *Ctenocardia fornicata* shell, (b) treated shell (S4), and sorbents (c) C1, (d) C2 (e) C3 and (f) C4.

Fig. 4 Zeta potential of treated *Ctenocardia fornicata* shell (S4) at (a) pH 6.4 (S4) and (b) pH 13.5.

Fig. 5 Transmission electron microscopy of sorbents: (a) C1, (b) C2, (c) C3; (d) C4.

Fig. 6 N₂ adsorption/desorption isotherms of (a) commercial CaO and sorbents (a) C1, (b) C2, (c) C3 and (d) C4.

Fig. 7 Pore size distribution curves of (a) commercial CaO and sorbents (a) C1, (b) C2, (c) C3 and (d) C4.

Fig. 8 CO₂ absorption performance (a) commercial CaO and sorbents (b) C1, (c) C2, (d) C3 and (e) C4.

Fig. 9 CO₂ desorption performance (a) commercial CaO and sorbents (b) C1, (c) C2, (d) C3 and (e) C4.

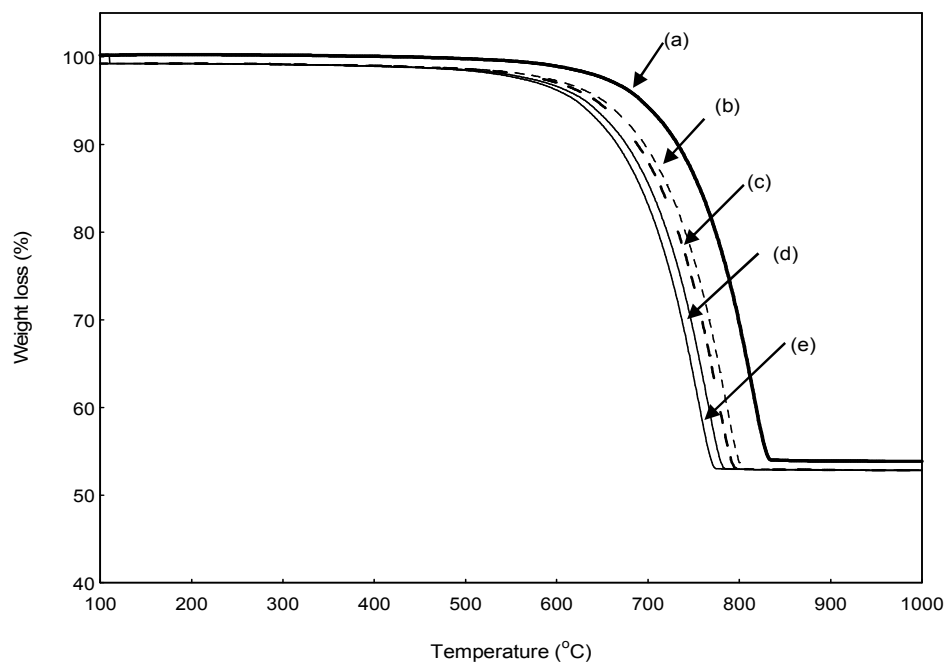


Fig. 1 TGA analyses of the powdered *Ctenocardia fornicata* shell (a) and treated shells: (b) S1 (c) S2, (d) S3 and (e) S4.

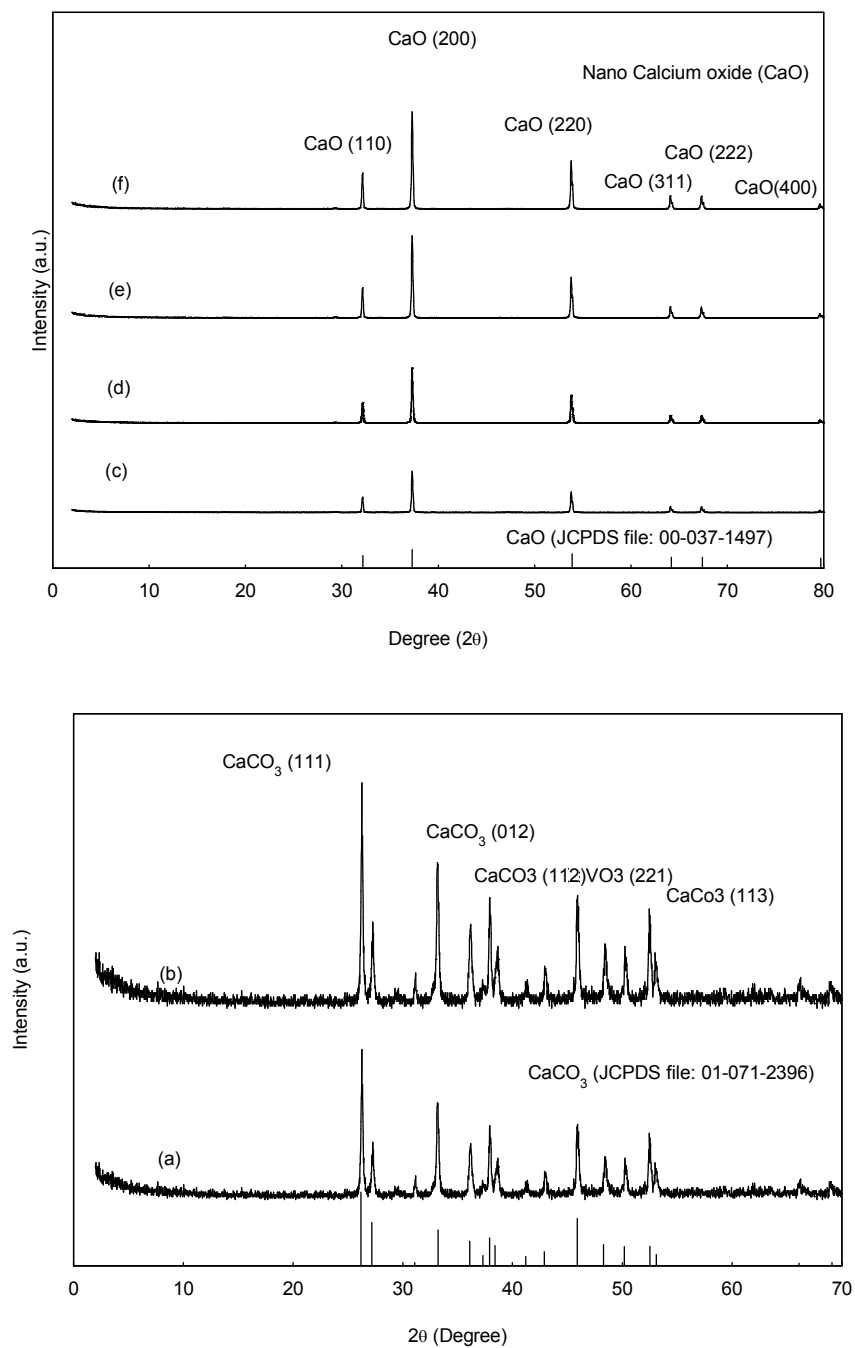


Fig. 2 X-Ray diffraction pattern of (a) *Ctenocardia fornicata* shell (b) treated shell (S4) and sorbents: (c) C1, (d) C2, (e) C3 and (f) C4.

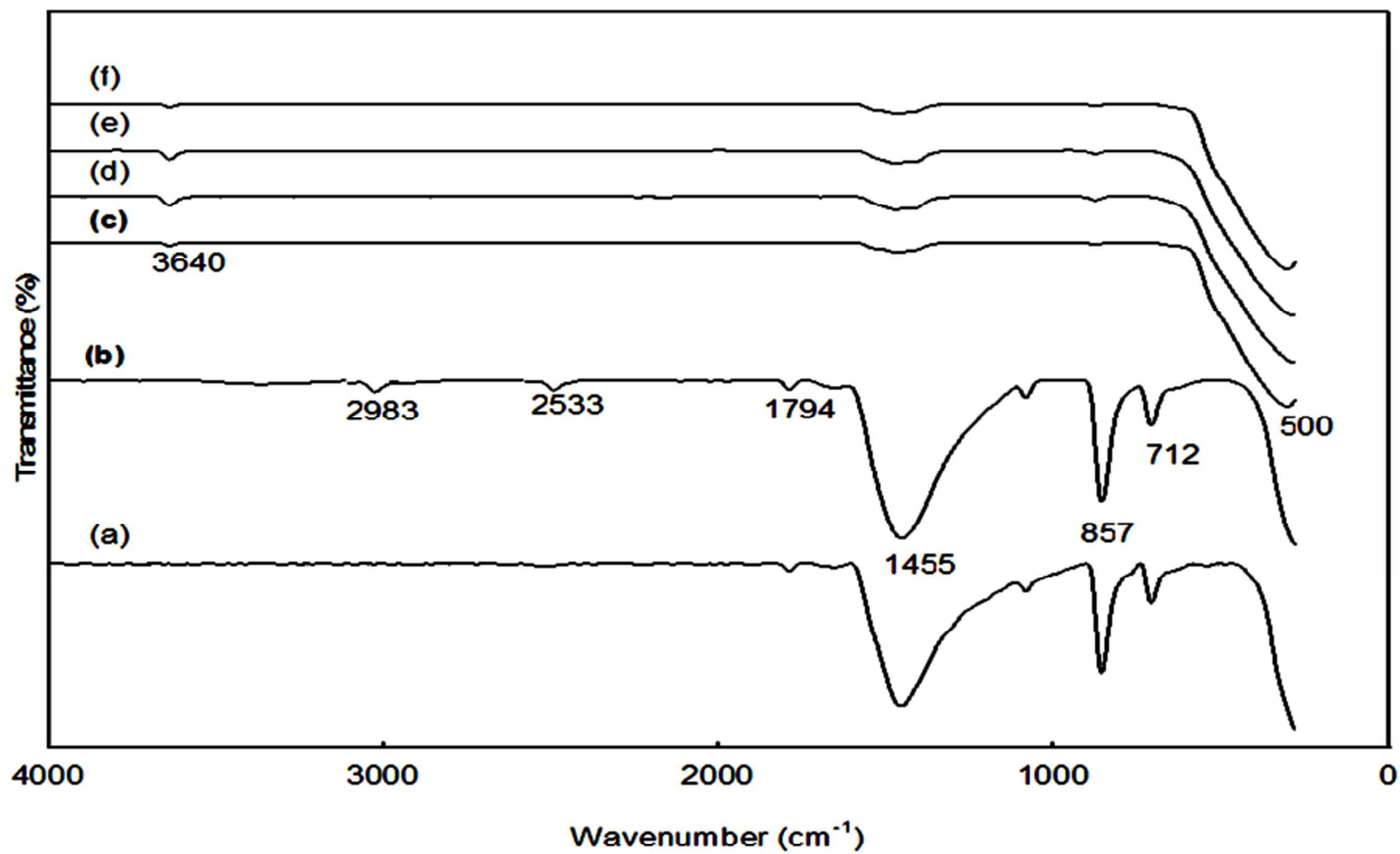


Fig. 3 FT-IR spectra of (a) *Ctenocardia fornicata* shell, (b) treated shell (S4), and sorbents (c) C1, (d) C2 (e) C3 and (f) C4.

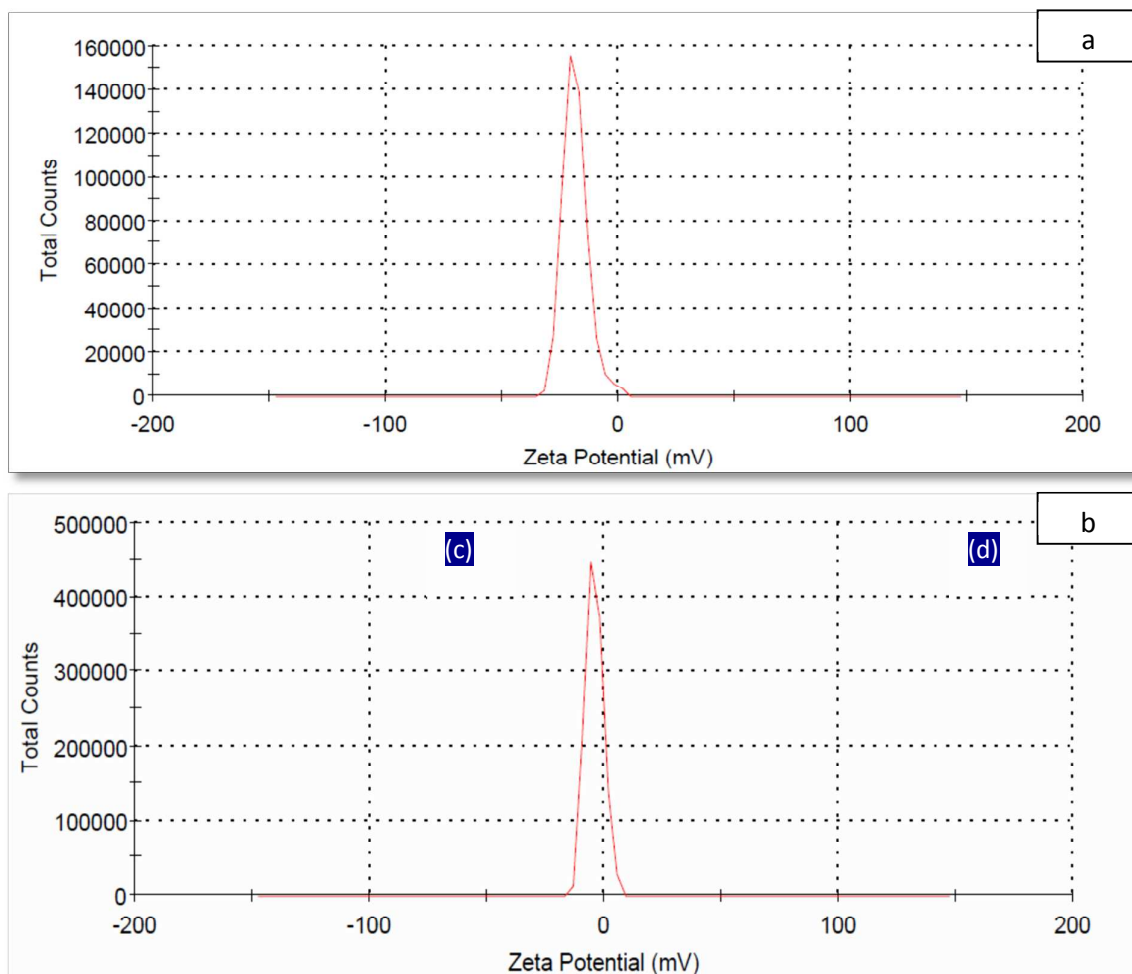


Fig. 4 Zeta potential of treated *Ctenocardia fornicata* shell (S4) at (a) pH 6.4 (S4) and (b) pH 13.5.

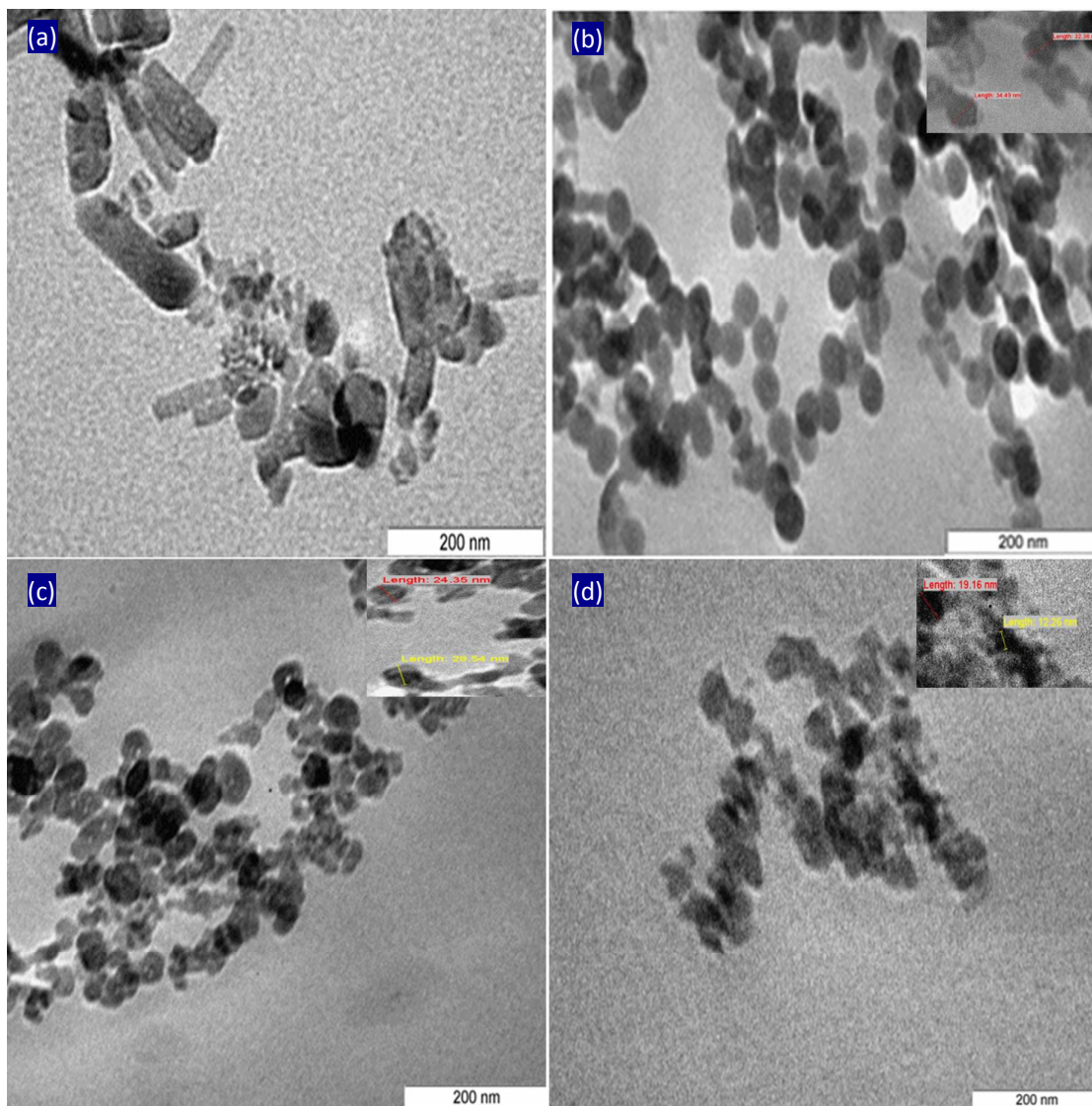
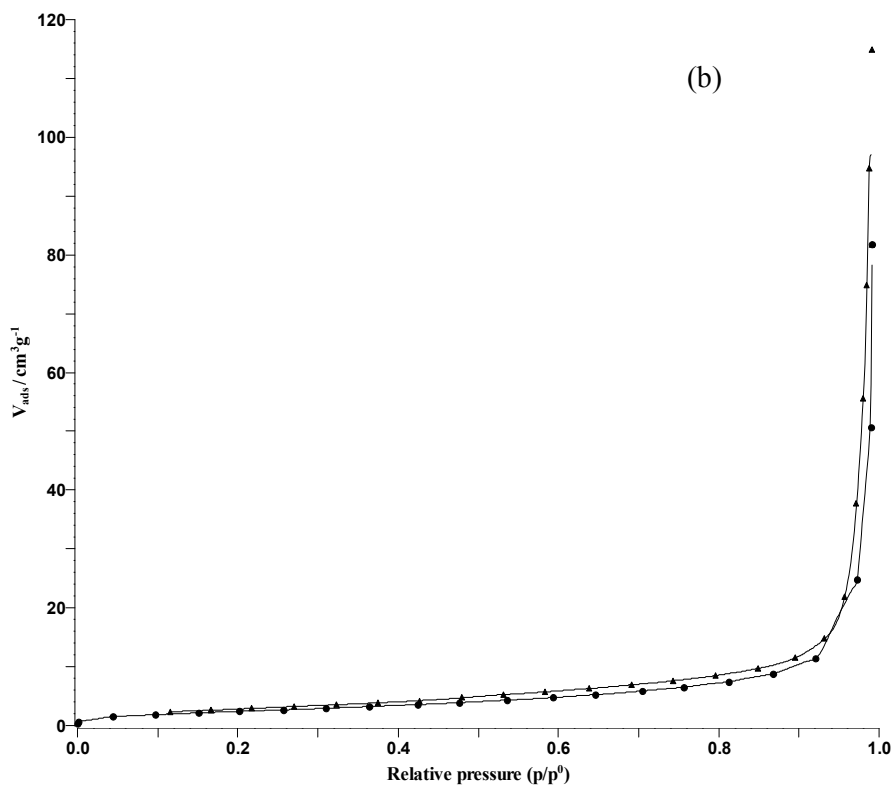
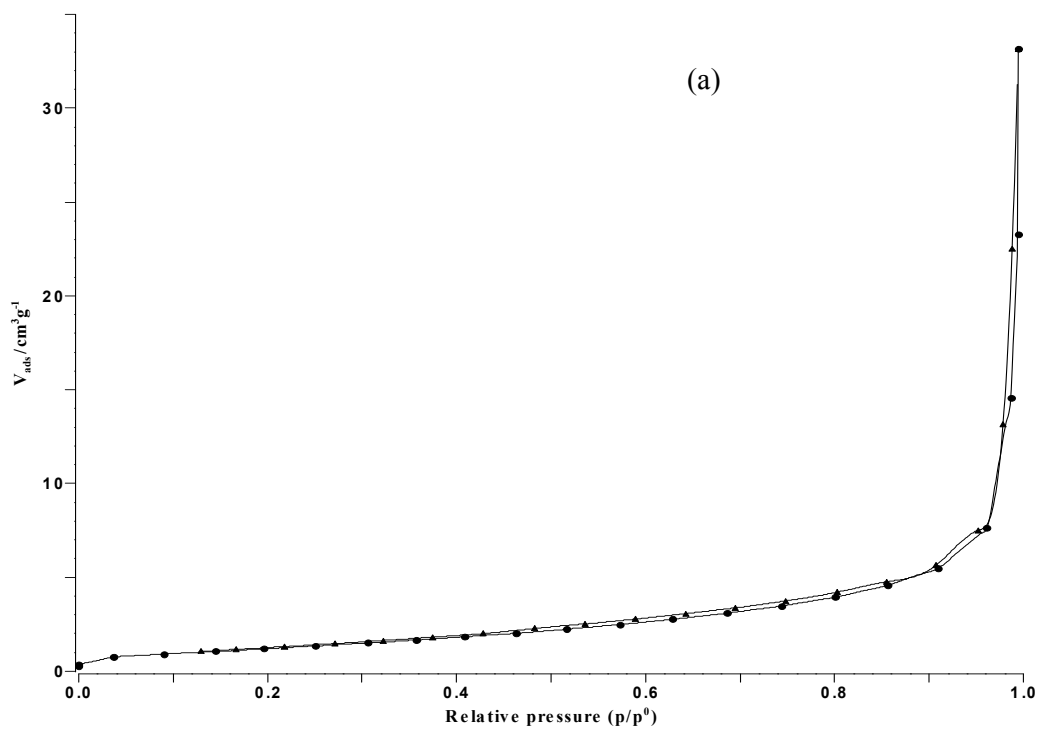
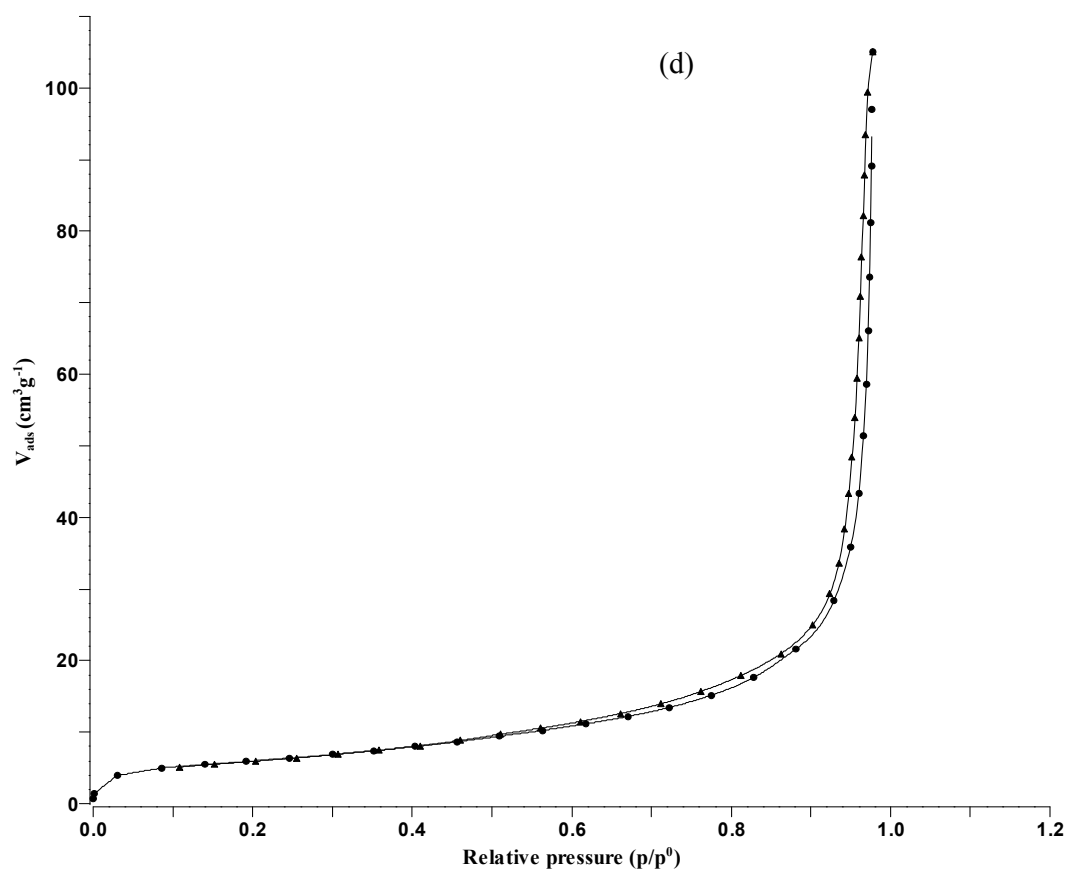
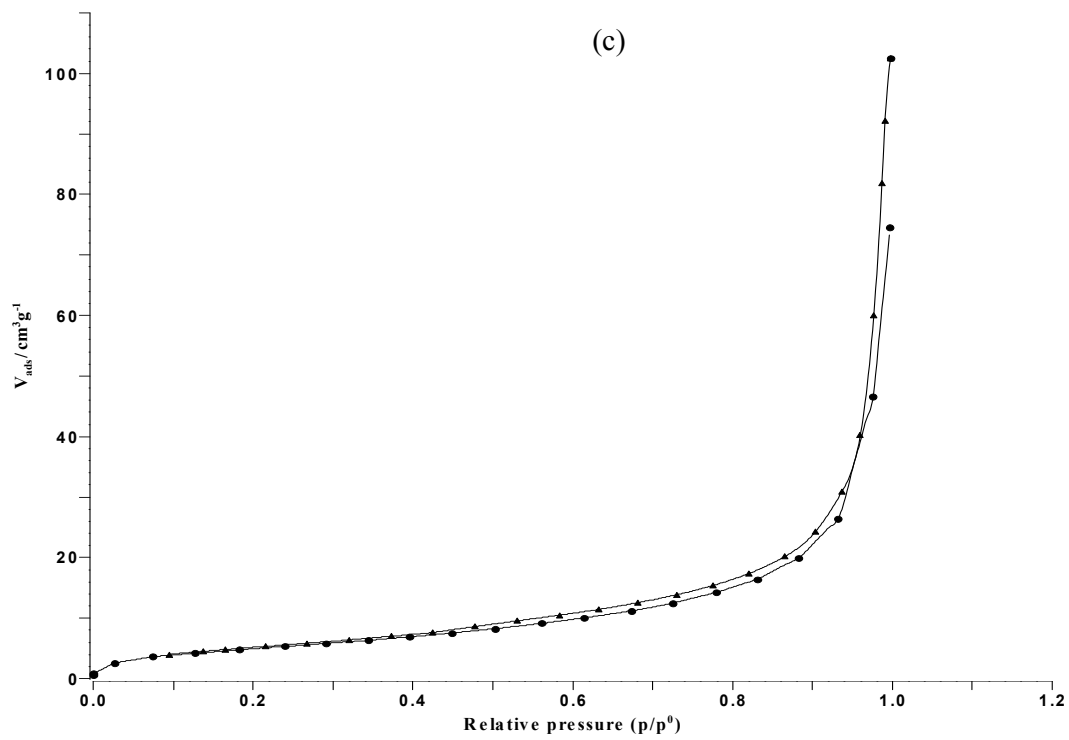


Fig. 5 Transmission electron microscopy of sorbents: (a) C1, (b) C2, (c) C3; (d) C4.





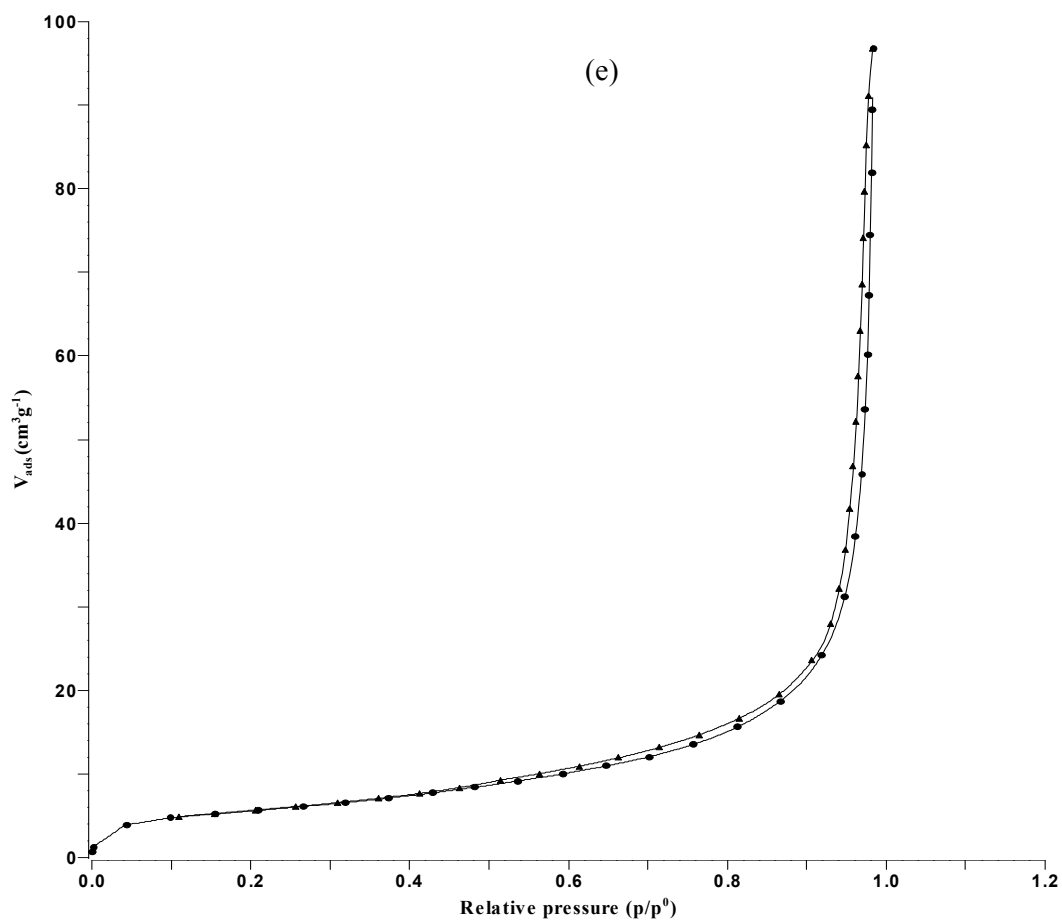
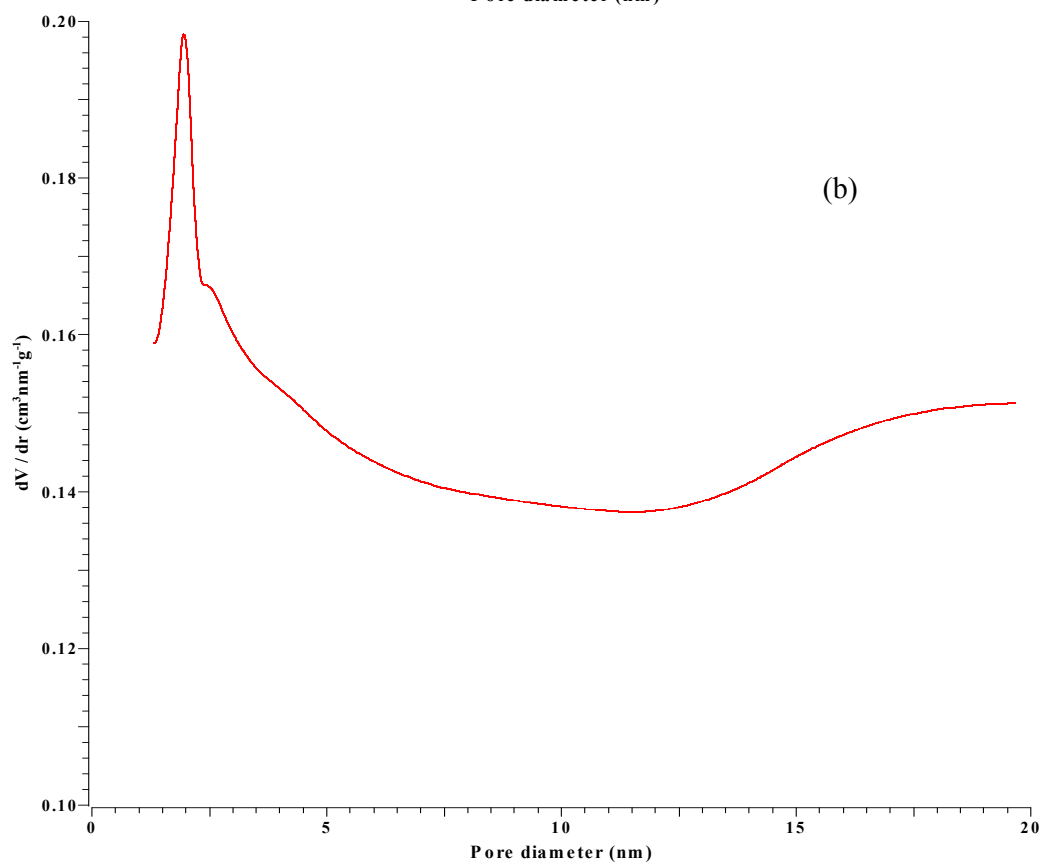
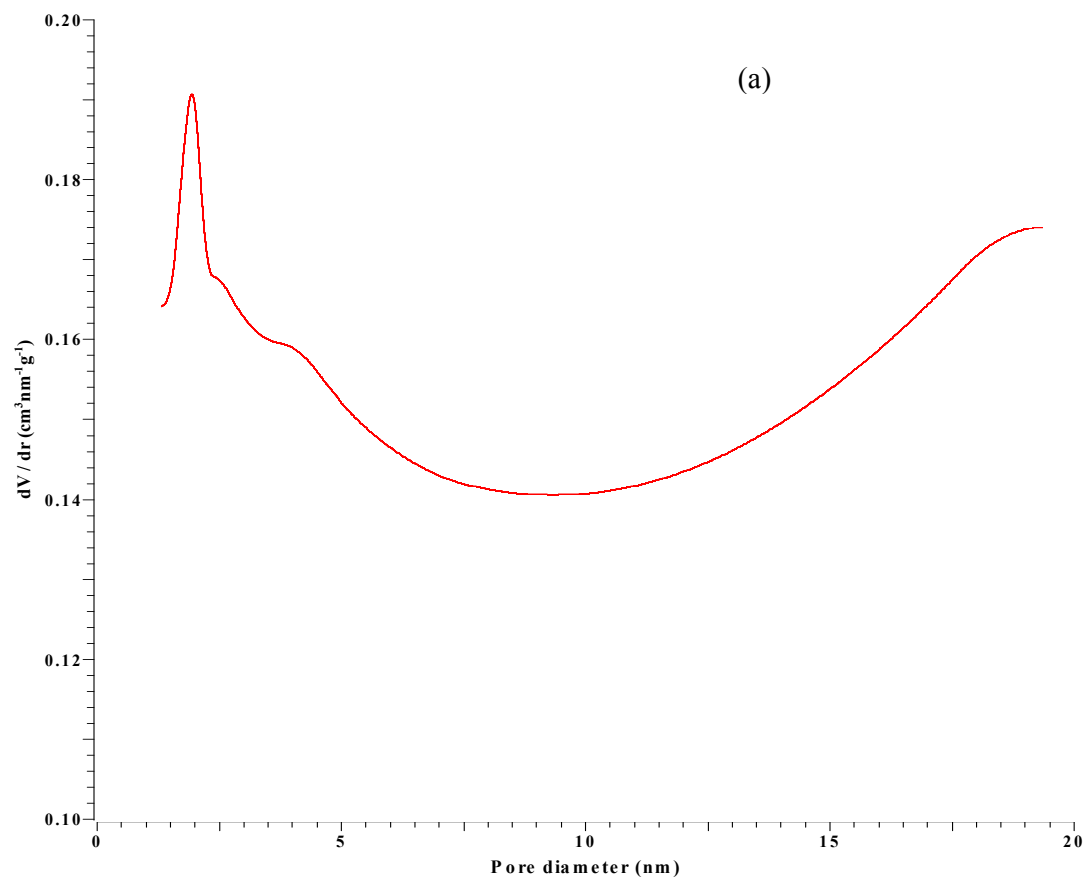
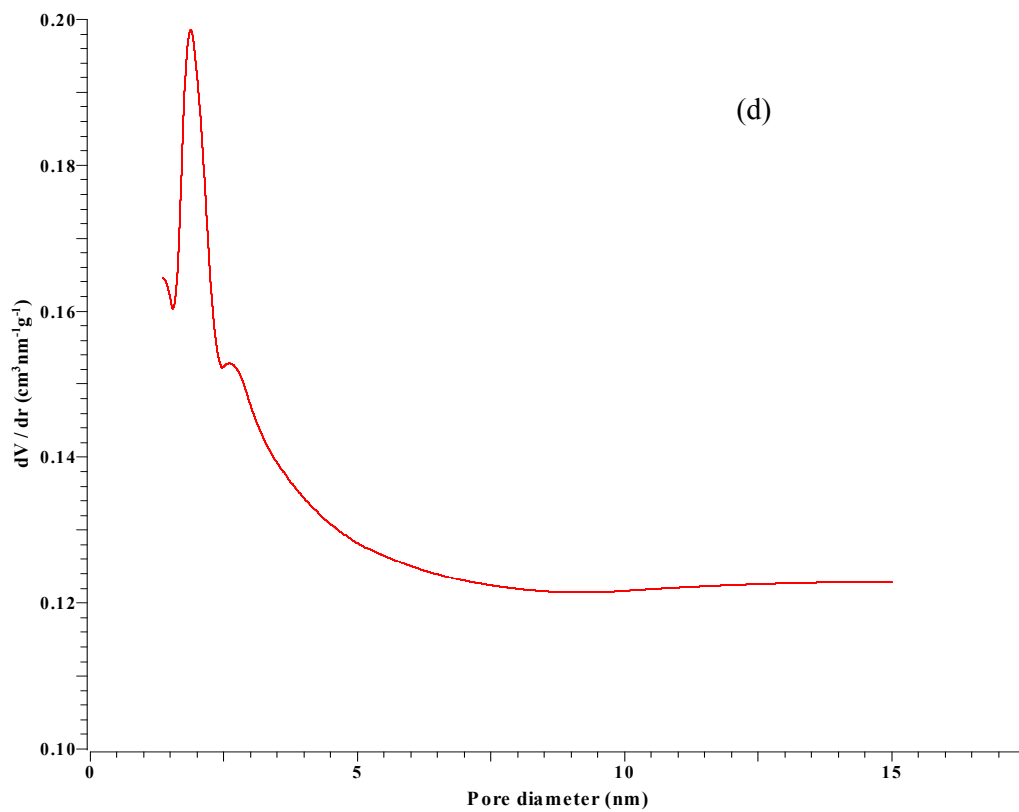
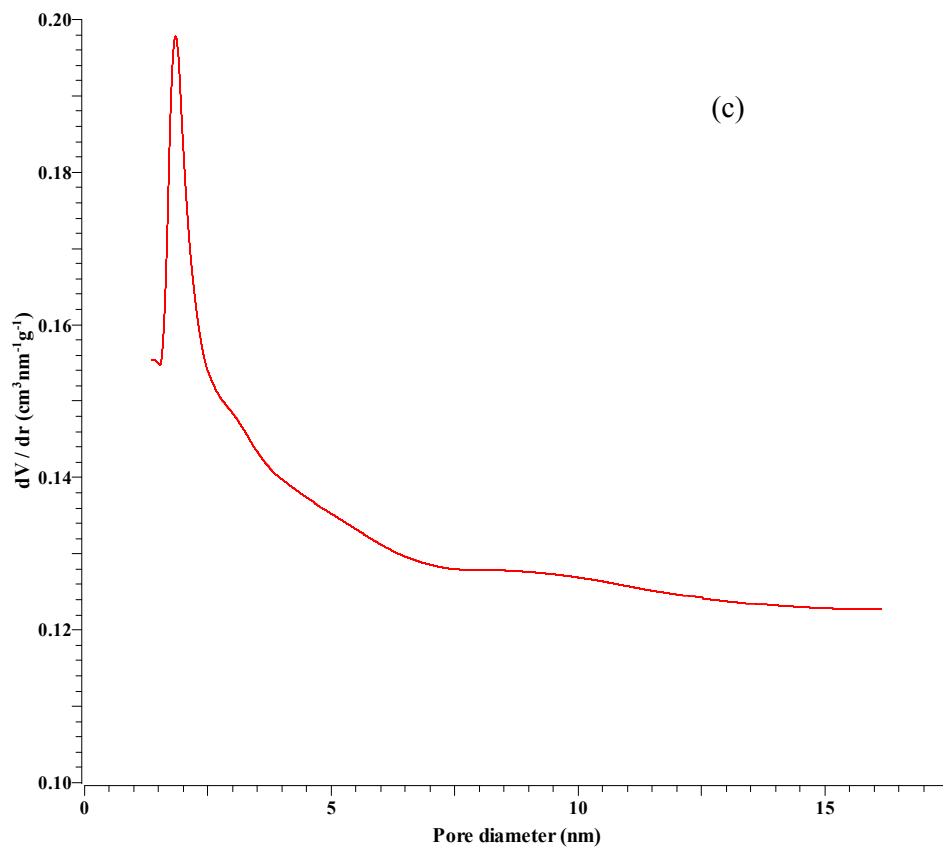


Fig. 6 N_2 adsorption/desorption isotherms of (a) commercial CaO and sorbents (a) C1, (b) C2, (c) C3 and (d) C4.





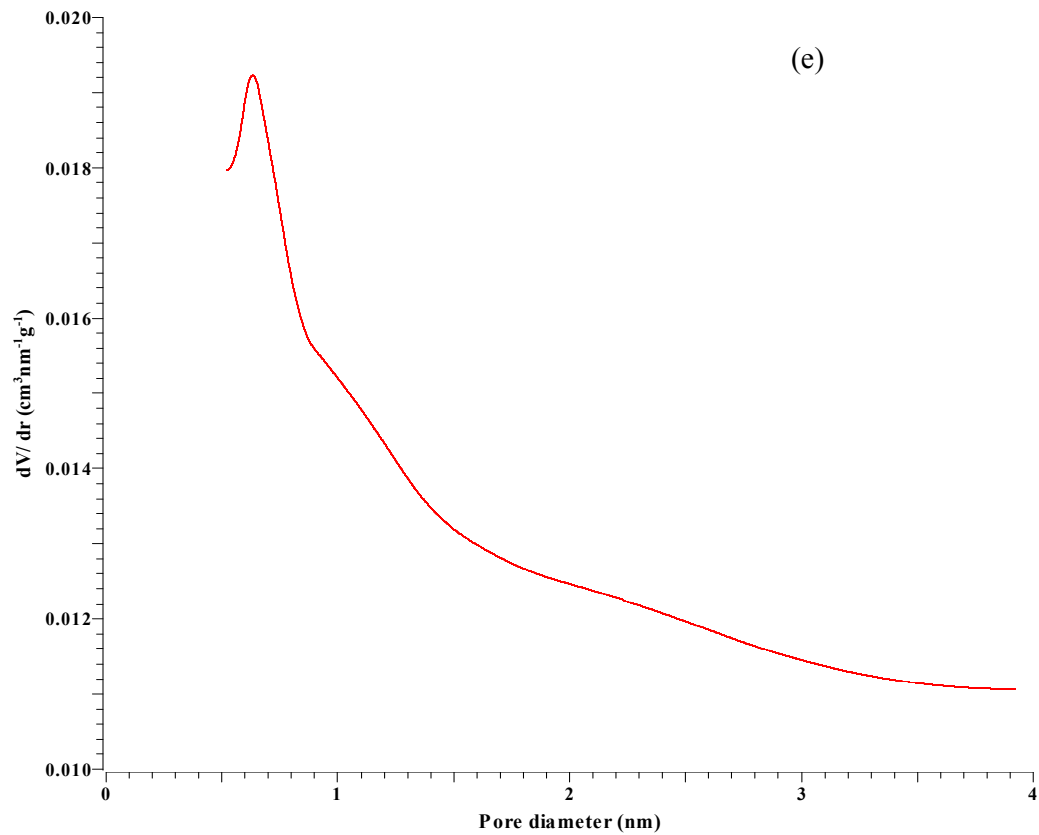


Fig. 7 Pore size distribution curves of (a) commercial CaO and sorbents (a) C1, (b) C2, (c) C3 and (d) C4.

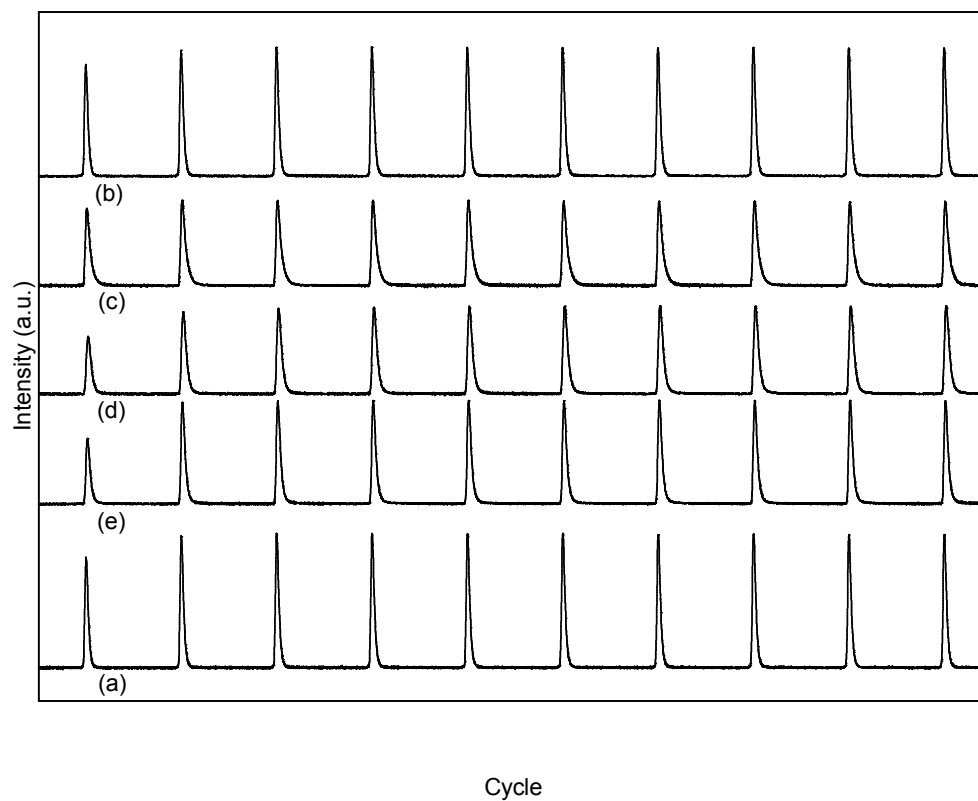


Fig.8 CO₂ absorption performance (a) commercial CaO and sorbents (b) C1, (C) C2, (d) C3 and (e) C4.

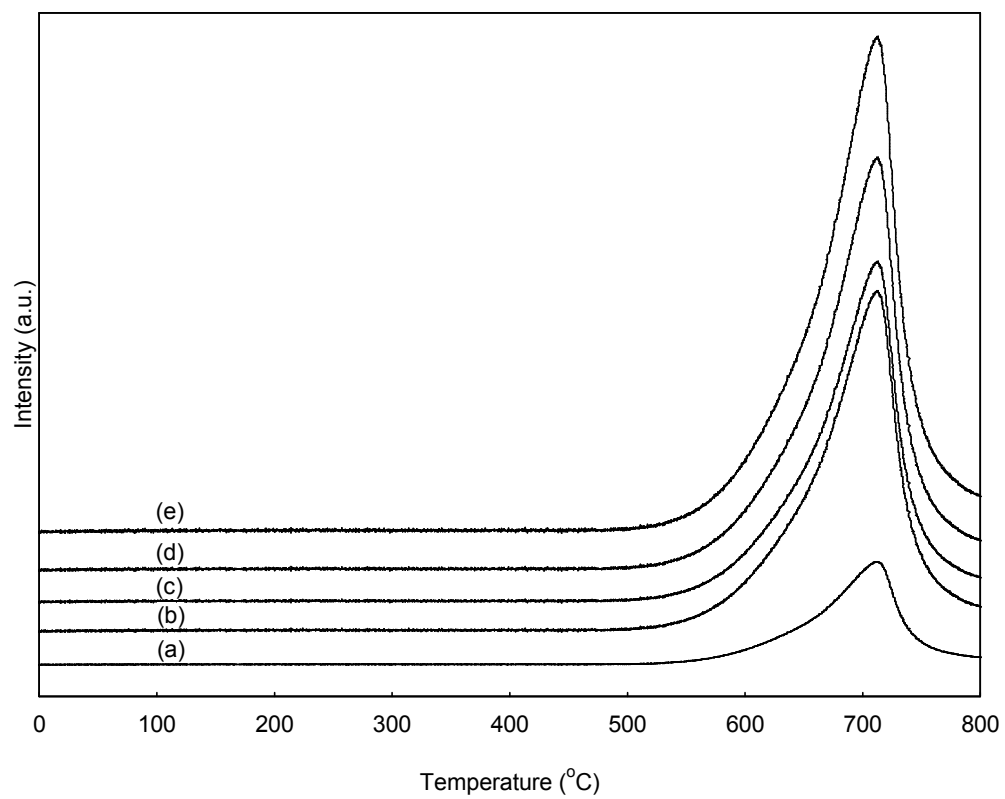


Fig. 9 CO₂ desorption performance (a) commercial CaO and sorbents (b) C1, (c) C2, (d) C3 and (e) C4.

Table captions

Table 1 Surface functional groups of *Ctenocardia fornicata* shell, treated shell and sorbents

Table 2 Chemical composition of *Ctenocardia fornicata* shell

Table 3 Zeta potential of *Ctenocardia fornicata* shell and treated shell

Table 4 BET surface area analysis of commercial CaO and sorbents

Table 5 The amount of CO₂ absorption and desorption of the sorbents

Table 1 Surface functional groups of *Ctenocardia fornicata* shell, treated shell and sorbents

Assignment	^a Peak position (cm ⁻¹)								
	3640 OH	2983	2533	1794 C=O	1455 CO ₃ ²⁻	1182 C-N	857 CO ₃ ⁻²	712 CO ₃ ⁻²	500 Others
<u>Sample</u>									
<i>Ctenocardia fornicata</i>	NA	NA	NA	w	s	m-s	s	m-s	s
S4	NA	w	w	w	s	m-s	s	m-s	s
C1	w	NA	NA	NA	w	NA	w	NA	s
C2	w	NA	NA	NA	w	NA	w	NA	s
C3	w	NA	NA	NA	w	NA	w	NA	s
C4	w	NA	NA	NA	w	NA	w	NA	s

^a s = strong, m = medium and w = weak intensities

NA= not found

Table 2 Chemical composition of *Ctenocardia fornicata* shell

Metal composition	Percentage (%)
Ca	99.3
S	0.345
K	0.238
Sr	0.082
Cu	0.048
Fe	0.027

Table 3 Zeta potential of *Ctenocardia fornicata* shell and treated shell

pH	Zeta potential (mV)	
	<i>Ctenocardia fornicata</i> shell	Treated sample (S4)
6.4	-18.61	-20.13
13.5	-11.13	-4.13

Table 4 BET surface area analysis of commercial CaO and sorbents

Composition	BET surface area ($\text{m}^2 \text{g}^{-1}$)	BJH desorption average pore diameter (nm)
Commercial CaO	4.7	10.62
C1	8.4	8.05
C2	10.8	6.23
C3	13.5	6.50
C4	23.7	2.26

Table 5 The amount of CO₂ absorption and desorption of the sorbents

Sample	Sorption (mol g ⁻¹)	
	Absorption ^a	Desorption ^b
Commercial CaO	256.17	245.33
C1	683.10	654.56
C2	783.93	703.77
C3	854.47	813.38
C4	1134.89	982.24

^aDetermined by chemisorption experiment^bDetermined by CO₂-TPD analysis

Graphic abstract

